Elliptic vortex patches: coasts and chaos

Andrew Crosby
Cambridge University

We investigate the interaction of ocean vortex patches with boundaries via the elliptic moment model of Melander, Zabusky & Stysek [13], under which vortex patches are approximated as elliptic regions of uniform vorticity. The interaction with a straight boundary is shown to reduce to the problem of an ellipse in constant strain, as previously investigated by Kida [9]. Interactions with more complicated geometries, where we might have expected the motion to be chaotic, are found to be constrained by an adiabatic invariant arising from a separation of time scales between the rotation of the patch and its motion along the coast. A couple of examples where the presence of a background flow does produce clear chaotic motion are also given. Finally a conformal mapping technique is developed to find the motion of vortex patches in geometries where the flow is not so easily calculated.

1 Introduction

In many problems in geophysical fluid dynamics the flows of interest are quasi-two dimensional due to the presence of rotation, stratification or shallow water, and a ubiquitous feature of such flows are large-scale vortex structures. Examples include the famous Red Spot of Jupiter's atmosphere, which is thought to be well approximated by the shallow water equations [3]. Closer to home the Atlantic Ocean plays host to Gulf Stream rings, which are rings of hot or cold water formed by an instability of the gulf stream (see Figure 1a), and also to Meddies, which are formed by the flow of regions of warm salty water from the Mediterranean into the Atlantic (see Figure 1b). Such structures are important for the transport of heat/salt across the Atlantic and, due to their relatively long life-times (O(years) in the case of meddies), will inevitably interact with ocean boundaries; indeed a study by Richardson & Tychensky [15] observed that meddies would interact with seamounts and could sometimes be observed to breakup in the process.

Previous work by Johnson and McDonald [8, 7] had mainly focused on the modelling of such ocean vortices as point vortices and analysing their paths around islands or past coastal gaps. To complement this work they did some contour dynamics calculations to look at the motion of an initially circular patch of vorticity in such situations. The project presented by Ted Johnson at the Woods Hole program was motivated by an observation during this earlier work that, where the point vortex motion had a separatrix, it ought to be possible to find chaotic motion of a patch of vorticity. The two problems presented by Ted were that of motion around a pair of islands (see Figure 2a) where the vortex patch might be expected to chaotically switch which island it goes around, and that of motion past a coastal gap where the vortex patch might either go through the gap or continue along the coast in a chaotic scattering problem (see Figure 2b).

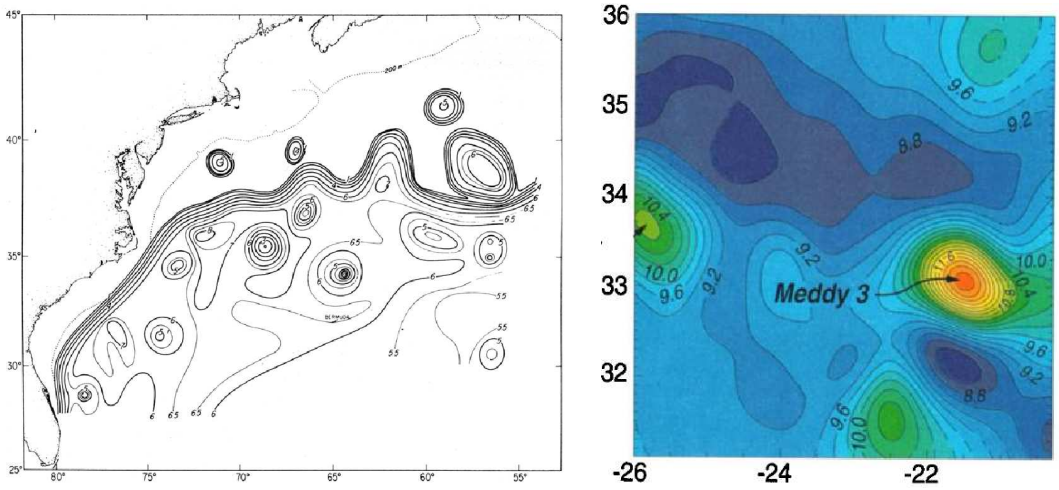

(a) Gulf stream rings visualized by depth in 100m of 15°C isotherm, (Richardson, Cheney & Worthington 1976) [14]

(b) Mediterranean eddies visualized by temperature at 1000m depth, (Richardson & Tychensky 1998) [15]

Figure 1: Examples of vortices present in the Earth's oceans

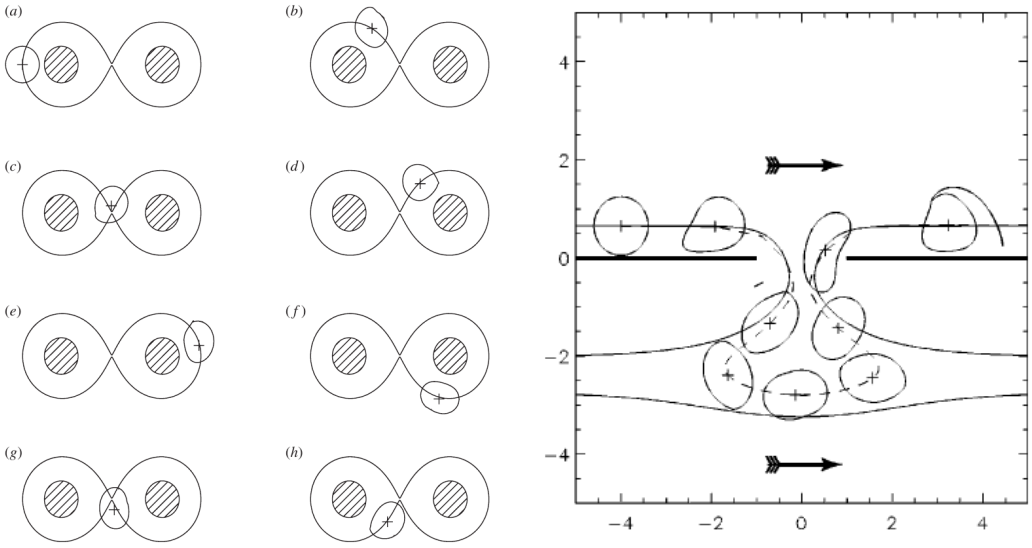

(a) Two islands.

(b) Coastal gap with background flow.

Figure 2: Contour dynamics simulations results by Johnson and McDonald where vortex patch shape could affect motion near a separatrix.

Figure 3: Approximation of vortex patches as ellipses under the moment model of MZS.

In the end there was only time to consider the problem of motion around a pair of islands but on route we discovered some interesting phenomena which are presented in the following sections.

2 Problem description

We consider the two-dimensional Euler equations, and model regions of vorticity as finite area patches of uniform vorticity. Under certain assumptions the motion of such patches is well approximated by an elliptic moment model developed by Melander, Zabusky & Stysek [13] (MZS from here on in). It is this model that we will utilise here so we begin by briefly describing the important results from its derivation.

2.1 Elliptic moment model

It is a remarkable result of Kirchoff [10] that an elliptic patch of vorticity in the absence of background flow maintains its elliptical shape and simply rotates about its centre. For a patch of vorticity ω and area A the rotation rate is given by

$$\Omega = \frac{\omega}{2 + r + r^{-1}} \tag{1}$$

where $r \geq 1$ is the ratio of the major axis to the minor axis of the ellipse. Furthermore such an elliptic patch remains elliptical under the application of some combination of uniform advection, rotation and strain. It is these results that form the backbone of the model of MZS.

It is worth noting that such elliptic vortex patches are not always stable: it was shown by Love [11] that for $r > 3$ the ellipse becomes unstable in the absence of any background flow, and Dritschel [4] extends this analysis to the case of an ellipse in a straining flow.

MZS considered a collection of uniform vorticity patches whose typical dimension, L, was much less than their typical separation, R. This separation allows the use of a multipole expansion when calculating the interaction between vortex patches. They then represented each vortex patch in terms of its centroid and Fourier modes representing the shape. At second order the model is particularly elegant as, under the extra assumption that the patches are initially approximately elliptical i.e. higher Fourier modes $\ll 1$, the model is

closed (requires no knowledge of higher moments). Thus the patches and their motion can be entirely represented in terms of their centroids and their elliptical shape.

Under these approximations patch centroids evolve due to the point vortex and elliptic moments from all the other patches. Meanwhile the elliptic shape of each patch evolves due to a self-contribution causing it to rotate (c.f. Kirchoff) and the strain flow generated by the point vortex contributions from the other patches.

2.2 Representing an ellipse

It is useful at this stage to consider a couple of methods for representing an elliptical shape, if we assume that the size of the ellipse is fixed then the shape needs two independent quantities to represent it. Perhaps the simplest and most physically intuitive is the following:

$$(r, \theta) \tag{2}$$

where $r \geq 1$ is the ratio of the major to minor axis and θ is the angle that the major axis makes to the horizontal. In the following sections it will often be convenient to represent the ellipse in terms of its quadrupole moment

$$\mathbf{q} \equiv \begin{pmatrix} q_{xx} & q_{xy} \\ q_{xy} & q_{yy} \end{pmatrix} \equiv \int (\mathbf{x} - \mathbf{x}_c)(\mathbf{x} - \mathbf{x}_c)\ dS \tag{3}$$

where $\mathbf{x}_c$ is the centroid of the ellipse and the integral is over the area of the ellipse. This can be written in terms of (r, θ) as follows:

$$\mathbf{q} = \frac{A^2}{4\pi} \begin{pmatrix} r\cos^2\theta + r^{-1}\sin^2\theta & (r - r^{-1})\sin\theta\cos\theta \\ (r - r^{-1})\sin\theta\cos\theta & r\sin^2\theta + r^{-1}\cos^2\theta \end{pmatrix} \tag{4}$$

There are only really two independent quantities here as $\det(\mathbf{q})$ is a function only of the area A and consequently is fixed. Finally we can also represent the ellipse via a complex quadrupole moment

$$q \equiv \int (z - z_c)(z - z_c)\ dS = (q_{xx} - q_{yy}) + 2iq_{xy} \tag{5}$$

where $z = x + iy$.

2.3 Hamiltonian representation

The underlying two-dimensional Euler equations are Hamiltonian and it was observed by MZS that their elliptic model preserved the Hamiltonian structure. Here we will sketch a derivation of the Hamiltonian in terms of complex variables, (the use of complex variables allows for a much more compact representation of the quadrupole interactions).

The Hamiltonian for the two-dimensional Euler equations is given by the excess energy [1]

$$H = -\frac{1}{2}\int \omega\psi\ dS - \int \omega\Psi\ dS \tag{6}$$

where ψ is the stream function due to the vorticity in the flow and Ψ is the stream function for an externally-imposed irrotational flow. For patches of uniform vorticity, and assuming no background flow for the time being, we can rewrite the above expression as

$$H = -\frac{1}{2}\sum_i \omega_i \int \psi_i \; dS_i - \frac{1}{2}\sum_{i\neq j} \omega_i \int \psi_j \; dS_i \tag{7}$$

where $\int \cdot \, dS_i$ is an integral over patch i, ω_i is the vorticity of patch i, and ψ_i is the stream function due to patch i.

The elliptic moment model of MZS is equivalent to integrating over elliptic regions, and expanding ψ_j in the second term as a multipole expansion while keeping terms up to order $(L/R)^2$.

The stream function due to a point vortex of unit strength at $\mathbf{x}_0$ is given by

$$\psi(\mathbf{x}) = -\frac{1}{2\pi}\log\left(|\mathbf{x}-\mathbf{x}_0|\right). \tag{8}$$

As the flow due to a point vortex is irrotational this can be written in terms of a complex stream function ϕ which is an analytic function of $z = x + iy$

$$\phi(z) = \frac{1}{2\pi i}\log(z - z_0) \tag{9}$$

from which the stream function can be recovered by taking the imaginary part.

The complex stream function due to patch i, ϕ_i can be written as

$$\phi_i(z) = \frac{\omega_i}{2\pi i}\int \log(z-\hat{z}) \; d\hat{S}_i, \tag{10}$$

which can then be expanded about the centroid of the patch z_i in a multipole expansion

$$\phi_i(z) \approx \frac{\omega_i}{2\pi i}\int \log(z-z_i) - \frac{\hat{z}-z_i}{z-z_i} - \frac{(\hat{z}-z_i)^2}{2(z-z_i)^2} \; d\hat{S}_i \tag{11}$$

the second term disappears as z_i is the centroid of the patch and the third term can be rewritten in terms of the complex quadrupole, q, defined earlier

$$\phi_i(z) \approx \frac{\omega_i}{2\pi i}\left(A_i \log(z-z_i) - \frac{q}{2(z-z_i)^2}\right). \tag{12}$$

The contribution to the Hamiltonian from the stream function of patch i evaluated at patch j in Equation (7) is calculated by expanding this multipole expansion as a quadratic around z_j

$$\phi_i(z) \approx \frac{\omega_i}{2\pi i}\left(A_i \log(z_j - z_i) - \frac{q_i}{2(z_j-z_i)^2} + \frac{A_i}{z_j - z_i}(z-z_j) - \frac{A_i}{2(z_j-z_i)^2}(z-z_j)^2\right) \tag{13}$$

and then integrating over patch j to give

$$\omega_j \int \psi_i \; dS_j = -\frac{\omega_i\omega_j}{2\pi}\,\mathrm{Re}\left(A_i A_j \log(z_j - z_i) - \frac{A_i q_j + A_j q_i}{2(z_j-z_i)^2}\right). \tag{14}$$

Calculation of the self-interaction term is more complicated and here we will just quote the result of MZS rewritten in terms of q:

$$\omega_i \int \psi_i \, dS_i = \frac{(\omega_i A_i)^2}{4\pi} \log\left(\frac{4\pi}{A_i^2}\sqrt{|q_i|^2 + \frac{A_i^4}{4\pi^2}} + 2\right). \tag{15}$$

These results can then be combined to give a full Hamiltonian

$$H = -\sum_i \frac{(\omega_i A_i)^2}{8\pi} \log\left(\frac{4\pi}{A_i^2}\sqrt{|q_i|^2 + \frac{A_i^4}{4\pi^2}} + 2\right) - \sum_{i\neq j} \frac{\omega_i \omega_j}{4\pi} Re\left(A_i A_j \log(z_j - z_i) - \frac{A_i q_j + A_j q_i}{2(z_j - z_i)^2}\right). \tag{16}$$

To complete the model we need to know how to obtain the equations of motion from the Hamiltonian: this can be achieved either by directly deriving the equations of motion and working backwards [13] or directly from the Hamiltonian Euler equations [12]. The resulting equations are as follows:

$$\dot{x}_i = \frac{1}{\omega_i A_i}\frac{\partial H}{\partial y_i} \tag{17}$$

$$\dot{y}_i = -\frac{1}{\omega_i A_i}\frac{\partial H}{\partial x_i} \tag{18}$$

$$\dot{q}_{xi} = \frac{4\sqrt{|q_i|^2 + \frac{A^4}{4\pi^2}}}{\omega_i}\frac{\partial H}{\partial q_{yi}} \tag{19}$$

$$\dot{q}_{yi} = -\frac{4\sqrt{|q_i|^2 + \frac{A^4}{4\pi^2}}}{\omega_i}\frac{\partial H}{\partial q_{xi}} \tag{20}$$

Finally we note that (q_x, q_y) do not form a canonical variable pair but MZS observe that the following pair, written here in terms of r and θ do.

$$\left(\frac{\omega_i A_i}{16\pi}\frac{(r_i - 1)^2}{r_i}, 2\theta_i\right) \tag{21}$$

3 Motion along a coast

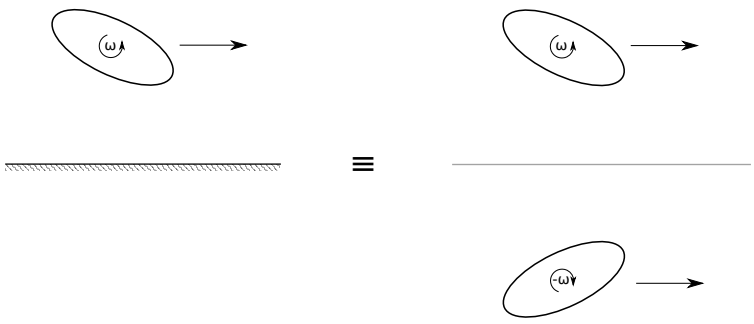

We begin by considering the simple case of a vortex patch moving along a coast or ocean-ridge. Consider the coast to lie along the line $y = 0$. This problem can be solved

via a simple image system: the motion is the same as that of two vortex patches where the image vortex is the reflection of the original vortex patch in the line $y = 0$. The image patch will have opposite vorticity and a quadrupole $\bar{q}$. Now from the previous section we can construct the Hamiltonian as follows:

$$H = -\frac{(\omega A)^2}{8\pi} \log\left(\frac{4\pi}{A^2}\sqrt{|q|^2 + \frac{A^4}{4\pi^2}} + 2\right) + \frac{\omega^2}{4\pi} Re\left(A^2 \log(z - \bar{z}) - \frac{A(q + \bar{q})}{2(z - \bar{z})^2}\right) \tag{22}$$

$$H = -\frac{(\omega A)^2}{8\pi} \log\left(\frac{4\pi}{A^2}\sqrt{(q_x^2 + q_y^2) + \frac{A^4}{4\pi^2}} + 2\right) + \frac{\omega^2}{4\pi}\left(A^2 \log(2y) + \frac{Aq_x}{4y^2}\right) \tag{23}$$

Applying equations (17) then gives the following evolution equations:

$$\dot{x} = \frac{\omega A}{4\pi y} - \frac{\omega q_x}{8\pi y^3} \tag{24}$$

$$\dot{y} = 0 \tag{25}$$

$$\dot{q}_x = -\frac{2\omega q_y}{2 + \frac{4\pi}{A^2}\sqrt{(q_x^2 + q_y^2) + \frac{A^4}{4\pi^2}}} \tag{26}$$

$$\dot{q}_y = \frac{2\omega q_x}{2 + \frac{4\pi}{A^2}\sqrt{(q_x^2 + q_y^2) + \frac{A^4}{4\pi^2}}} - \frac{A\omega}{4\pi y^2}\sqrt{(q_x^2 + q_y^2) + \frac{A^4}{4\pi^2}} \tag{27}$$

The first thing to notice is that the vortex patch stays at a fixed height above the wall; this is a consequence of the conservation of the y-component of the global centroid. Under the elliptic model the strain experienced by the patch comes only from the point vortex contribution of the image, this is of fixed magnitude and at a fixed distance hence the patch experiences a constant strain rate. This problem of an elliptic patch of vorticity in constant strain has previously been analysed by Kida [9]. By writing q_x and q_y in terms of r and θ we can rewrite the Hamiltonian in a form similar to that given in the paper of Kida

$$H = -\frac{\omega^2 A^2}{8\pi} \log(r + r^{-1} + 2) + \frac{\omega^2 A^2}{4\pi} \log(y) + \frac{\omega^2 A}{16\pi y^2}\frac{A^2}{4\pi}(r - r^{-1}) \cos(2\theta) \tag{28}$$

and then defining e to be the constant strain rate

$$e \equiv \frac{A\omega}{8\pi y_c^2} \tag{29}$$

we have the following for some constant c (dependant on H):

$$\cos(2\theta) = \frac{\omega}{e}\frac{r}{r^2 - 1} \log\left(\frac{(r+1)^2}{cr}\right). \tag{30}$$

Kida showed that there were three types of motion possible: rotation, nutation and extension in which respectively either the major axis of the ellipse oscillates about $\theta = 0$, the major axis continually rotates, or the ellipse gets stretched out indefinitely. For $\frac{e}{\omega} > 0.15$ the only possible motion is extension where the ellipse is stretched indefinitely (see Figure 4).

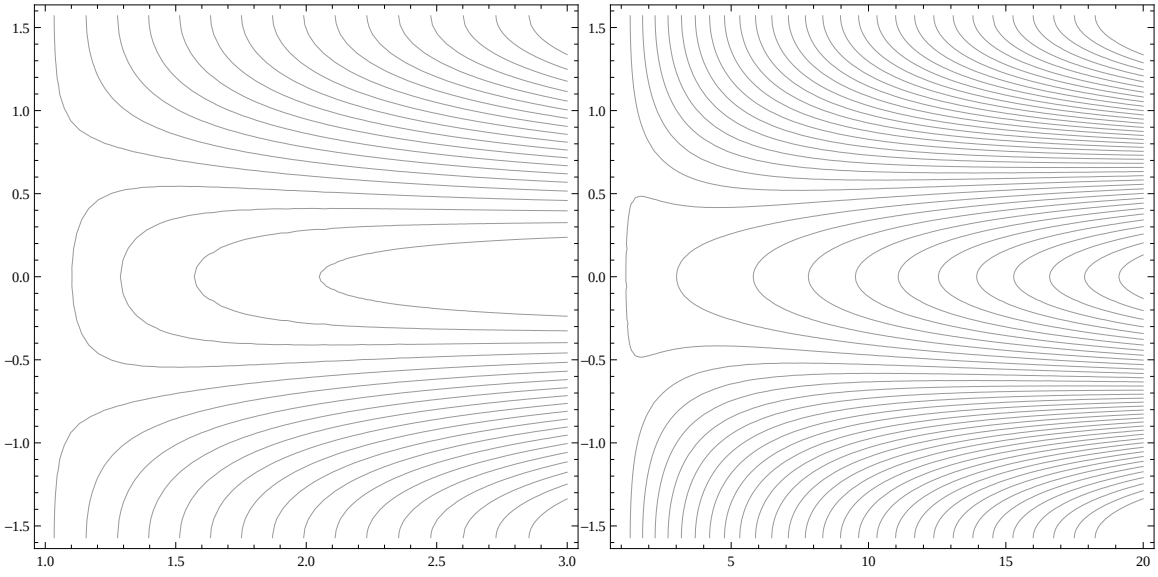

(a) (b)

Figure 4: $\frac{e}{\omega} = 0.2$. Contour plots of 2θ vs r.

For our value of e this corresponds to $A > 3.8y^2$ which for a circle would give radius $> 1.2y$. So when vortex patches are sufficiently close to a coast we expect them to break up, although we must be a little careful here because we have assumed that the vortex patch and its image are separated by a large distance in the model derivation so we can not expect this value to be quantitatively correct. There is a small range, $0.15 > \frac{e}{\omega} > 0.13$, where both nutation and extension are possible, and then for $\frac{e}{\omega} < 0.13$ all three types of motion can occur (see Figure 5).

3.1 Comparison with contour dynamics code

The full solution for the evolution of a patch of uniform vorticity can be calculated numerically using the method of contour dynamics [16]. This method makes use of the fact that the velocity only needs to be known on the boundary in order to evolve the patch position and that the velocity on the boundary can be calculated by an integral round the boundary as follows:

$$\nabla\psi(\mathbf{x}) = -\frac{1}{2\pi}\int \nabla_{\mathbf{x}} \log(|\mathbf{x}-\hat{\mathbf{x}}|)\; d\hat{S} \tag{31}$$

$$= \frac{1}{2\pi}\int \nabla_{\hat{\mathbf{x}}} \log(|\mathbf{x}-\hat{\mathbf{x}}|)\; d\hat{S} \tag{32}$$

$$= \frac{1}{2\pi}\int \log(|\mathbf{x}-\hat{\mathbf{x}}|)\; d\hat{\mathbf{n}}. \tag{33}$$

A comparison between the model and contour dynamics calculations is shown in Figure 6, here the patch has a unit radius and its centroid starts at a distance 1.5 above the coast. The model and full solution agree very well at early times but at later times there

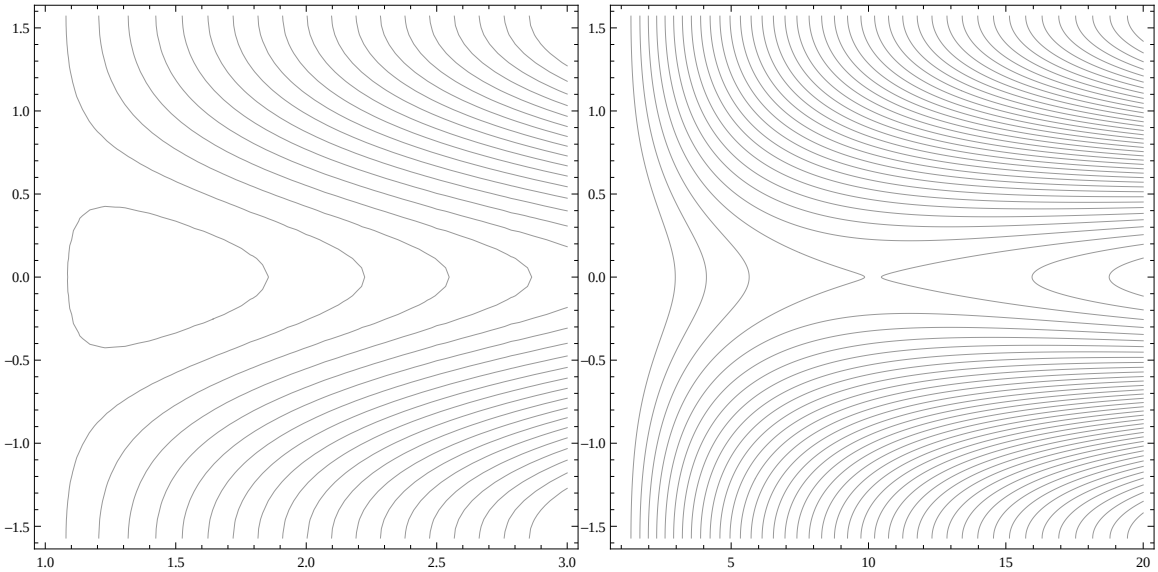

(a) (b)

Figure 5: $\frac{e}{\omega} = 0.08$. Contour plots of 2θ vs r.

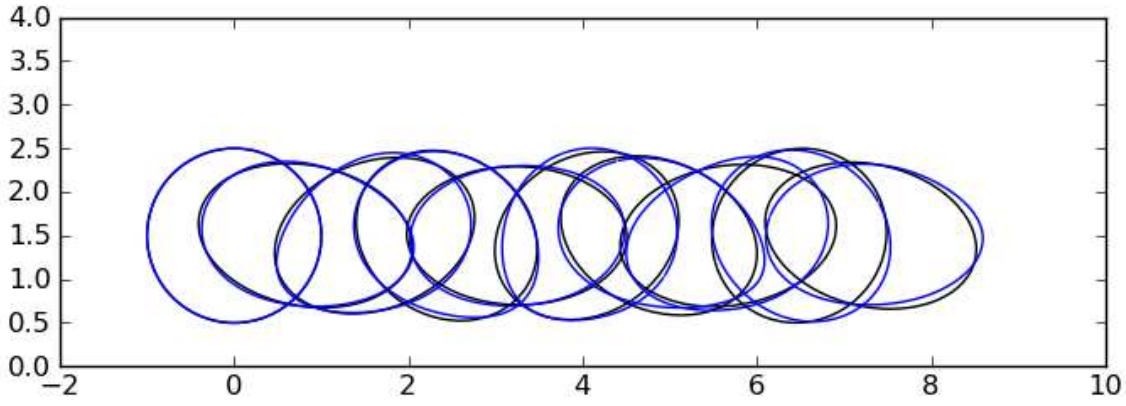

Figure 6: Motion of an initially circular patch with centroid at $y = 1.5$. Patch motion is from left to right with time intervals of $5/\omega$. Contour dynamics solution is in blue and the model in black.

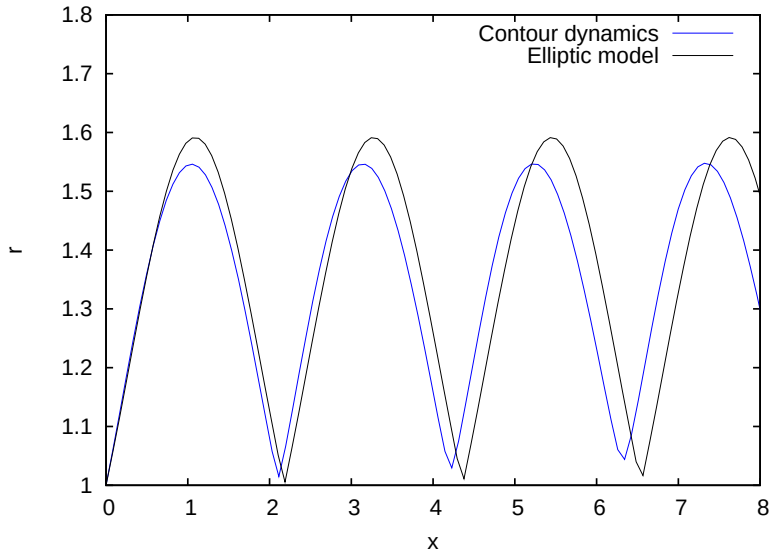

Figure 7: r against x for an initially circular patch with centroid at $y = 1.5$. For the contour dynamics solution r is calculated from the quadrupole moment.

is a noticeable phase drift. A more quantitative comparison is made in Figure 7, which again clearly shows the phase drift by also shows that the elliptic model overestimates the maximum value of r by $\sim 10\%$.

The good agreement between the model and full solution when $y = 1.5$, despite the technical requirement in the model derivation for the patch and its image to be well separated, raises the question of what happens if we use the model to calculate the motion of a patch of vorticity right next to the wall. The result of such calculations is shown in Figure 8. Whilst the elliptic model is clearly unable to capture the formation of a cusp it still does a remarkably good job of predicting the overall shape.

3.2 Background tide

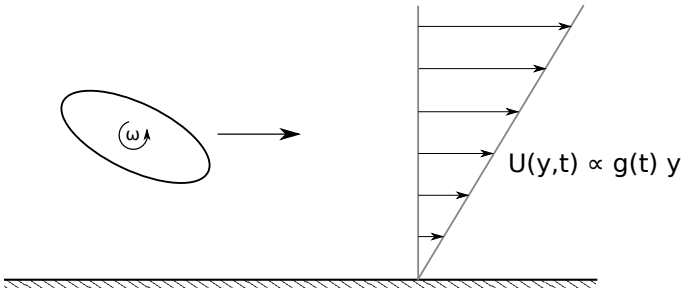

A natural extension to the previous problem is to ask what happens if there is a background flow along the coast. We consider here what happens if a time dependent background shear flow is imposed

$$U(y,t) = g(t)y \tag{34}$$

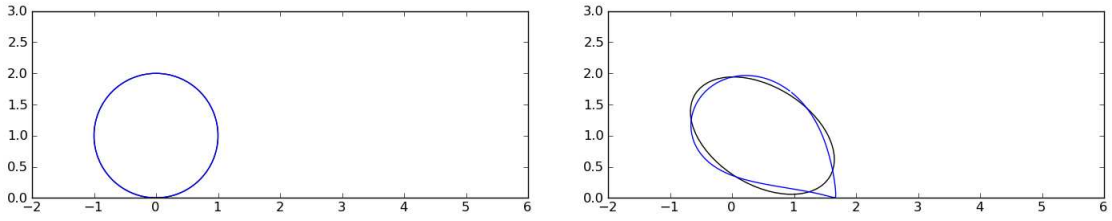

(a) $t = 0$ (b) $t = 2/\omega$

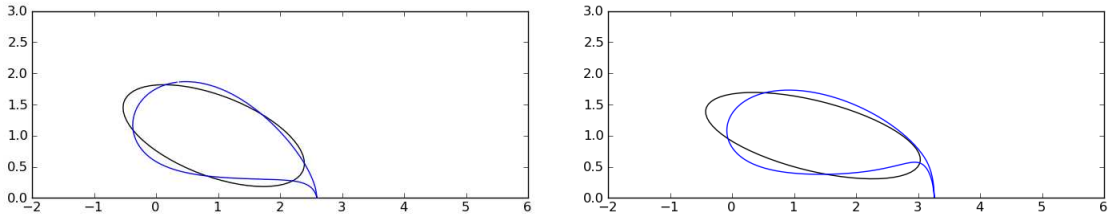

(c) $t = 4/\omega$ (d) $t = 6/\omega$

Figure 8: Even when the vortex patch is right next to the wall and consequently the model (black) should be completely invalid it still does a remarkably good job of capturing the overall shape of the region of vorticity (blue).

where we take the strength of the shear to vary sinusoidally with time

$$g(t) = f \sin\left(\frac{2\pi t}{T}\right). \tag{35}$$

Such shear might be caused by the presence of a tidal flow along the coast. It is known that, in the absence of a boundary, such background flows lead to chaotic behaviour [5].

We have to be a little careful when constructing the Hamiltonian for the motion of the elliptic patch in this flow as the background flow has infinite energy and is being driven by some unmodelled mechanism. The extra term that we add is

$$H_{shear} = -\omega \int \Psi_{shear}\, dS \tag{36}$$

where Ψ_{shear} is the (non-irrotational) stream function for the background flow

$$\Psi_{shear} = g(t)\frac{y^2}{2} \tag{37}$$

consequently we find that

$$H_{shear} = -\frac{\omega g(t)}{2}(Ay^2 + q_{yy}). \tag{38}$$

By neglecting any contribution due to the energy in the background flow we are effectively assuming that the background flow is unaffected by the presence of the vortex patch.

As the Hamiltonian is now time dependent we expect to find chaotic behaviour. The patch will still remain at a fixed height above the wall but we find more interesting behaviour if we consider what happens to the shape of the patch; the motion is now determined by three parameters: f, T and the initial distance from the wall y_0 (unless otherwise stated we will take $A = \pi$ and $\omega = 1$).

As an example we focus on the case of $y_0 = 3$. The unforced behaviour ($f = 0$) for this case is shown in Figure 9, for this value of y_0 almost all the orbits in the range of interest are rotations. We will consider what happens when we apply forcing with a period $T = 14$, from Figure 9b we see that this corresponds to the time period of an orbit with $r \approx 2$ when $\theta = 0$. Figures 10a & 10b show Poincaré sections of the resulting motion with points plotted every period T (the quantities plotted are actually the earlier canonical variables (Equation (21)) relabelled in terms of r and θ).

Initially a weak forcing of $f = 0.001$ is applied and a resonance opens up about the orbit with matching period (Figure 10a). In fact a similar resonance opens up about every orbit whose time period is a rational multiple of the forcing [2], but for this weak forcing they are too small to be observable here. An increase in forcing by a factor of 10 to $f = 0.01$ does little to affect the motion apart from increasing the size of the resonance (Figure 10b). As the forcing is increased further to $f = 0.05$ many of the higher order resonances become visible (Figure 11a). Finally by $f = 0.1$ a 'sea of chaos' has emerged (Figure 11b).

The development of resonances could have an impact on whether vortex patches are likely to break up: a sufficiently large resonance can take a vortex patch that is initially near circular and extend it well beyond $r = 3$ where the elliptic patch would become unstable in the absence of background flow. Similarly the emergence of a 'sea of chaos' allows the vortex patch to access all states within a large region of the Poincaré section including some for which the value of r is very large.

We can also consider what happens when the frequency of the forcing is changed: Figure 12 shows a Poincaré section when the forcing has a period of $T = 30$. One notable new feature here is that the sea of chaos that exists for most of the region $r \gtrsim 4$ extends out into a region where elliptic patches get extended indefinitely; this is why there aren't many points plotted in it as any solution that started there typically only survived a few periods before being indefinitely extended. This Poincaré section also provides us with an opportunity to observe one of the fundamental building blocks of chaos: the 'heteroclinic tangle' (see Figure 12b). When $f = 0$ we have a two-dimensional Hamiltonian system where the only type of fixed points are centres or saddles. A saddle point consists of the intersection of a stable and unstable manifold; in a two dimensional Hamiltonian system these manifolds can only intersect at a fixed point. However this saddle point structure is unstable and once a perturbation is added (here by increasing f away from zero) the two manifolds will typically intersect at a point away from the fixed point. The iterates of such an intersection lead to an infinite number of intersections away from the fixed point. On top of this the area-preserving property of a Poincaré section means that the area of the 'nodes', the regions formed by the two manifolds between intersections, must all be the same. Consequently as the intersections approach the fixed point the nodes get increasingly stretched out until eventually they start to wrap all the way around and overlap the fixed point in the perpendicular direction. It is this 'stretching' and 'folding' that guarantees the presence of a Smale Horseshoe and consequently chaotic behaviour. The presence of such

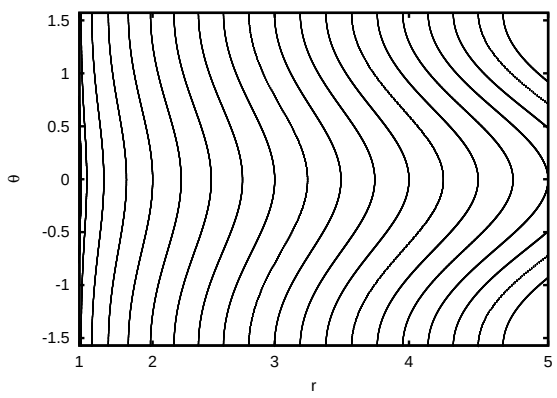

(a) Motion in the (r, θ) plane.

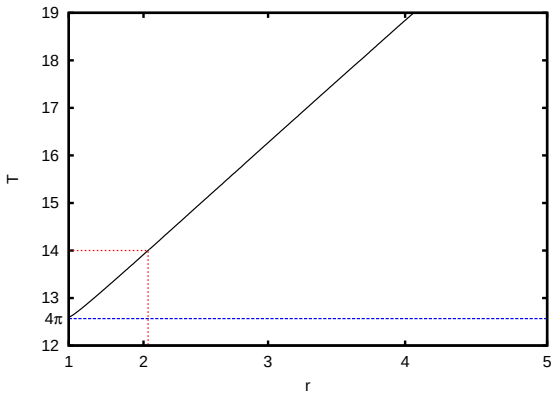

(b) Time period of orbits labelled by value of r at $\theta = 0$. The orbit times are all greater than that of an isolated circular patch for which $T = 4\pi$.

Figure 9: Behaviour for $y_0 = 3$ in the unforced case ($f = 0$).

tangles was predicted by Poincaré before we had the ability to calculate such structures numerically!

Finally we note that if the period of the forcing applied is much less or greater than the characteristic period associated with the rotation of the elliptic patch then, unless the forcing is very strong, the motion remains near integrable.

4 Motion around a corner

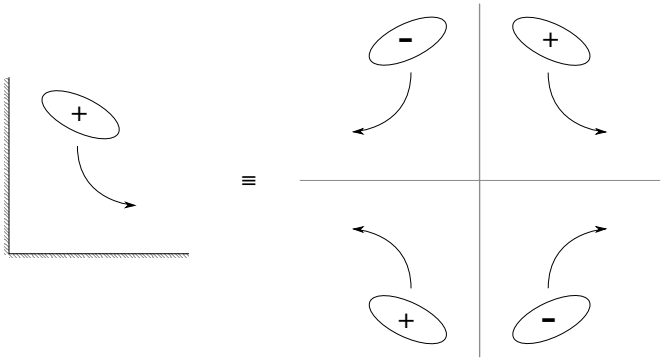

In the case of a patch moving above a straight coast the presence of a second conserved quantity (y component of the global centroid) meant the motion remained integrable. We will now consider what happens when a patch of vorticity moves in a quarter plane for which this extra conserved quantity does not exist. Far away from the corner the patch will remain at a constant distance from the coast but then the interaction with the corner will allow the distance to change. As this is a four-dimensional system we would expect to find chaotic behaviour.

We can again use the method of images (this time we need three images) to construct

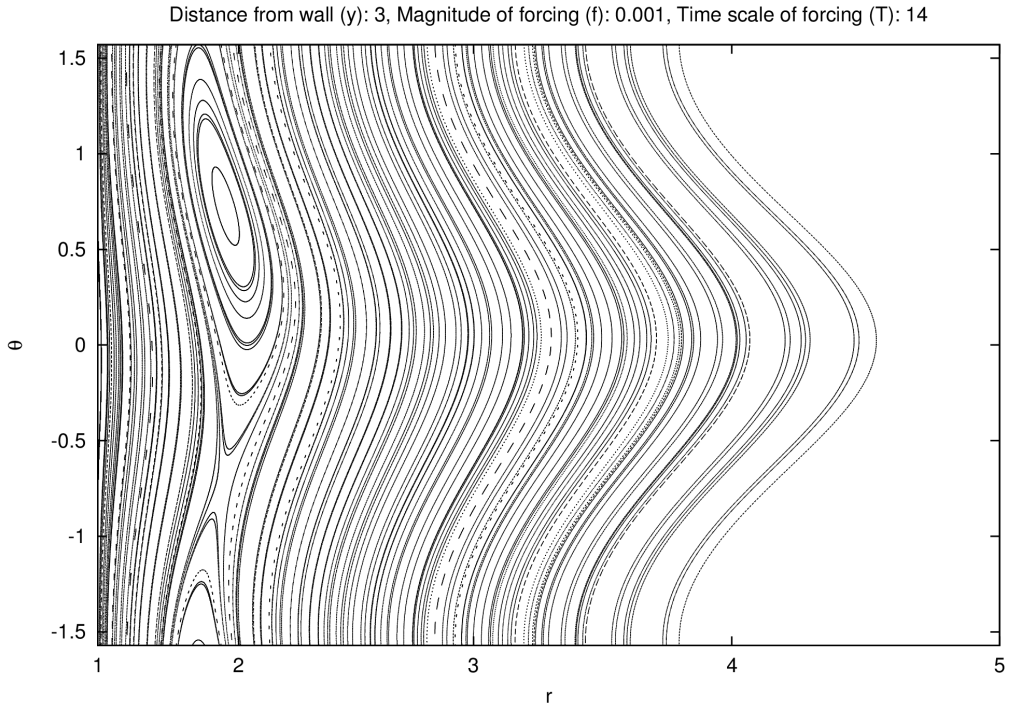

(a) $f = 0.001$

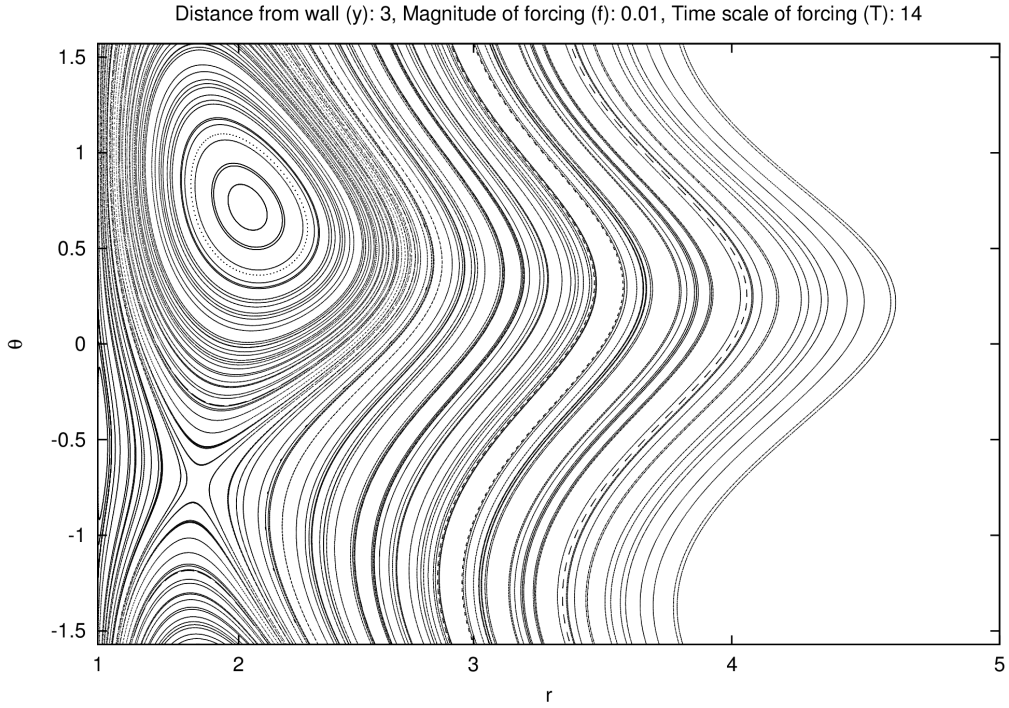

(b) $f = 0.01$

Figure 10: Poincaré sections for $y_0 = 3$, $T = 14$.

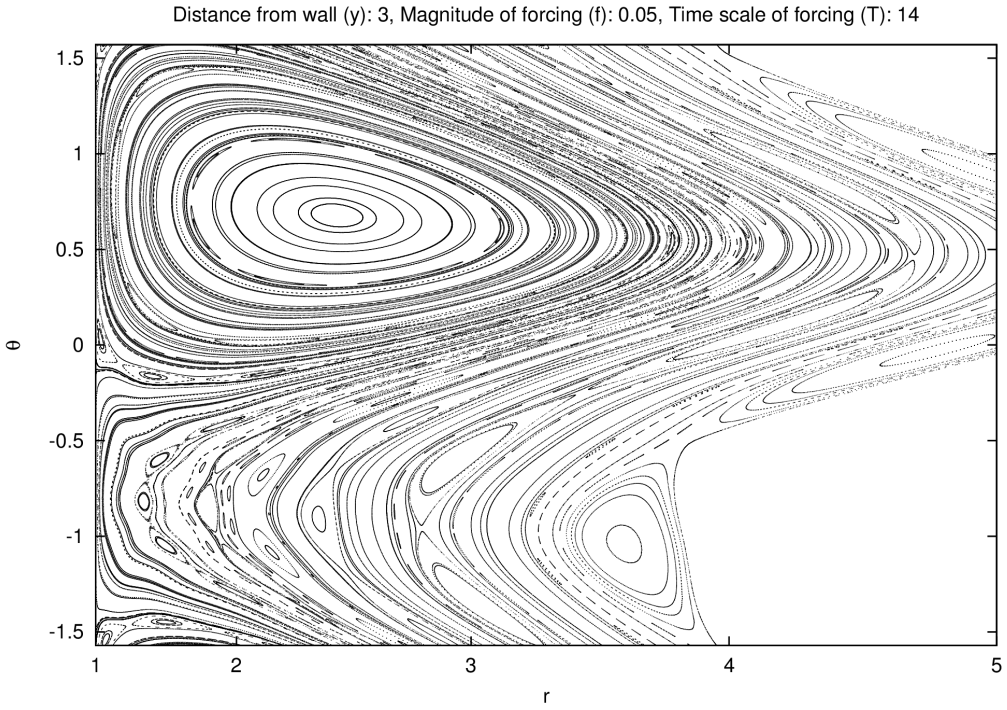

(a) $f = 0.05$

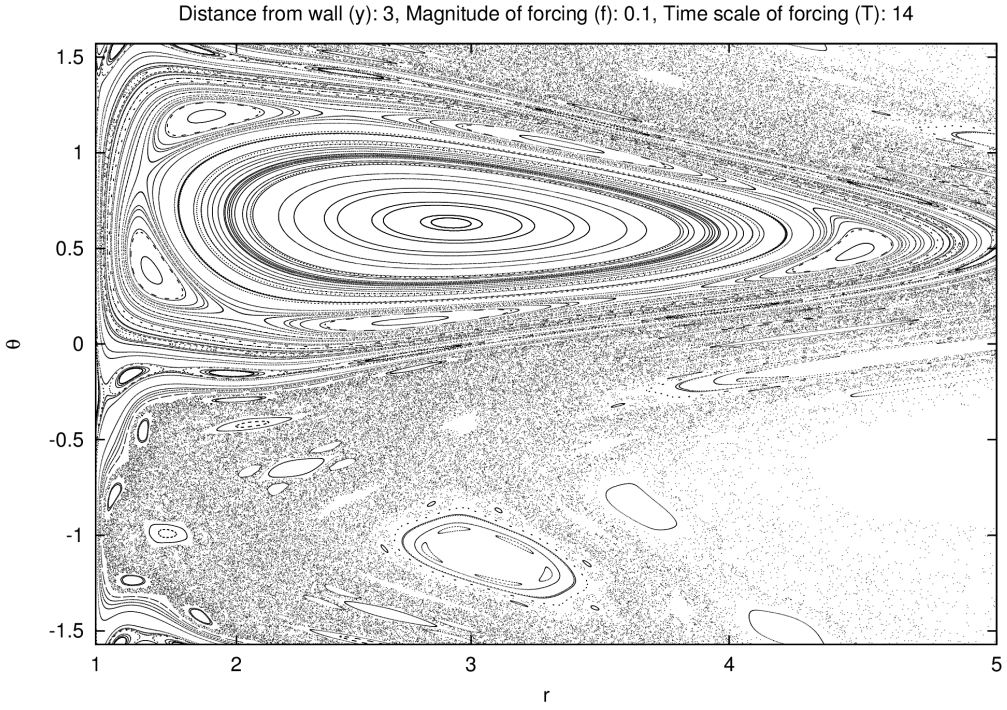

(b) $f = 0.1$

Figure 11: Poincaré sections for $y_0 = 3$, $T = 14$.

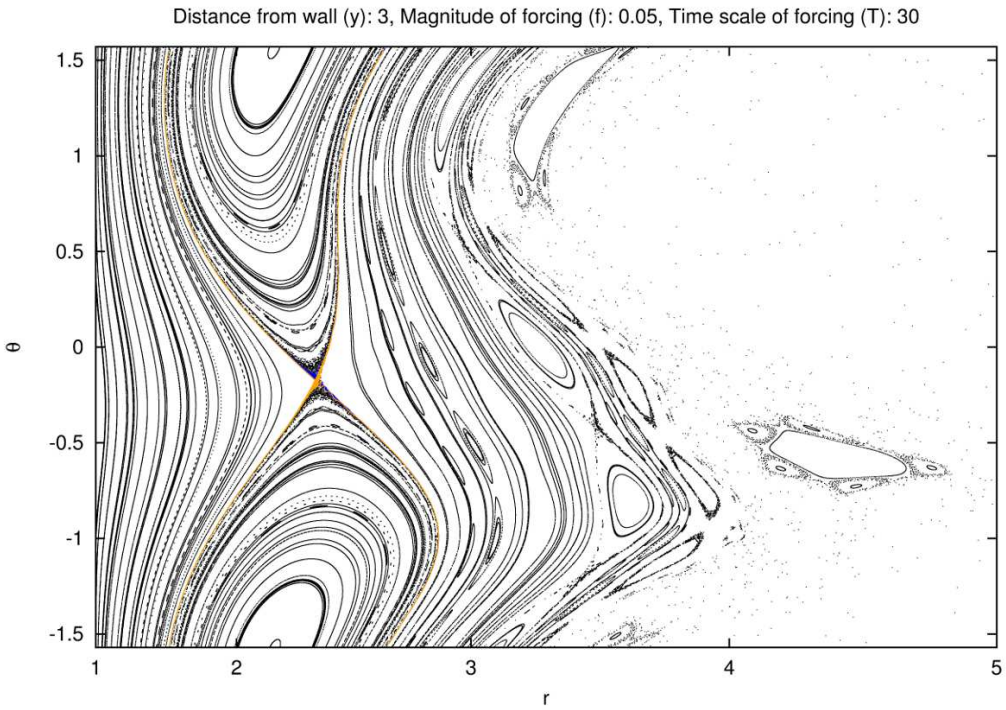

(a)

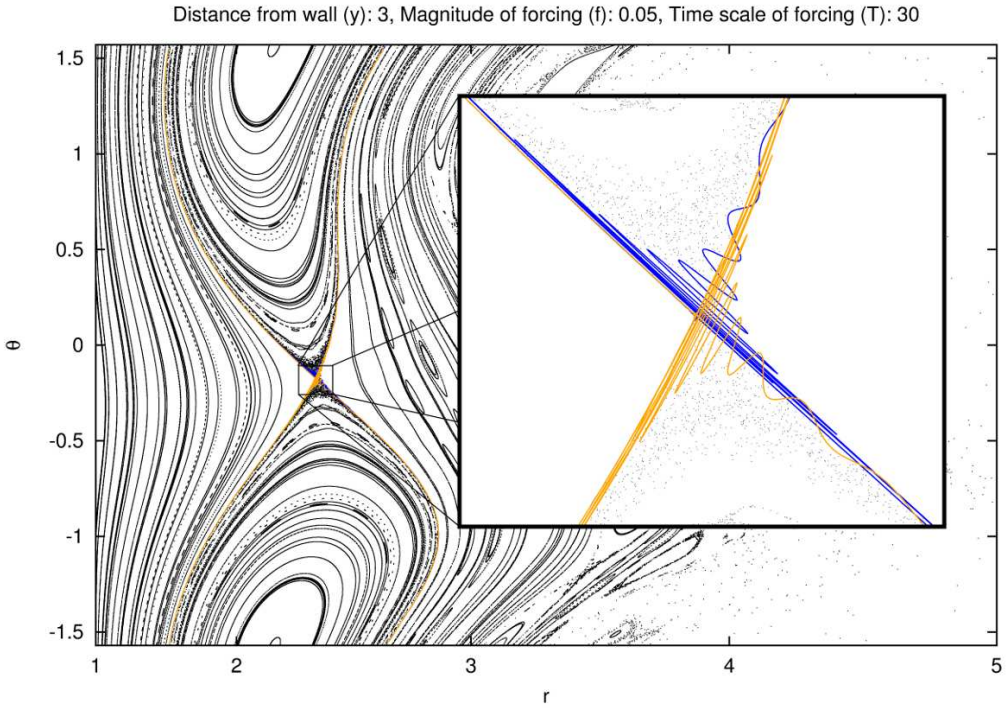

(b) Magnification of heteroclinic tangle.

Figure 12: Poincaré sections for $y_0 = 3$, $T = 30$, $f = 0.05$.

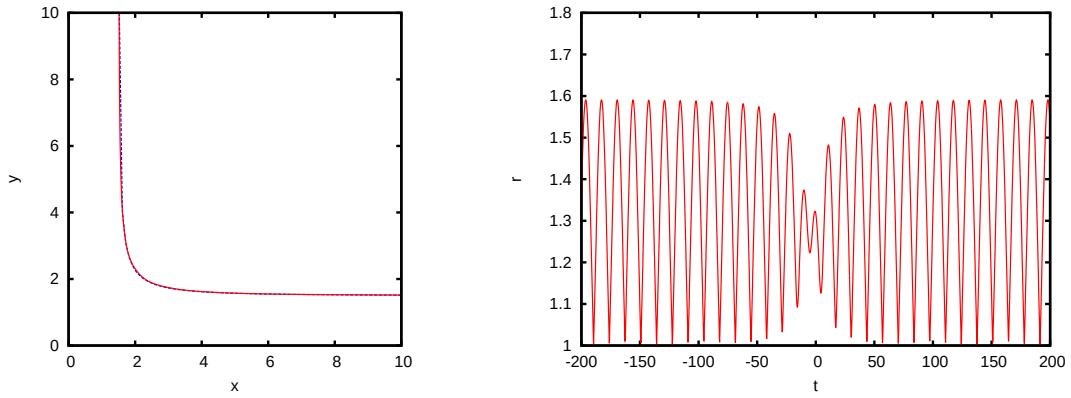

(a) Path of centroid in x-y plane.

(b) Variation of r with t.

Figure 13: Typical behaviour of a vortex patch moving round a corner. Initial conditions are $x = 1.5$, $y = 100$, $r = 1$ & $\theta = 0$.

the Hamiltonian

$$H = H_{self} + \frac{\omega^2}{4\pi}\left(A^2 \log(\frac{2xy}{\sqrt{x^2+y^2}}) + \frac{Aq_x}{4y^2} - \frac{Aq_x}{4x^2} + \frac{A(q_x(x^2-y^2)+2q_yxy}{4(x^2+y^2)^2}\right) \tag{39}$$

from which the motion of patches is easily calculated. Figure 13 shows an example of the resulting motion; the distances from the wall before and after the corner are very similar and consequently so is the behaviour of the elliptic shape. This example is typical and, unless patches are started so close to the wall that they extend indefinitely, all patches exit the corner at a similar distance from the wall as they entered, with the maximum deviation being of order 10^{-4}.

The explanation for this surprising behaviour comes from considering the time scales involved in the problem: there is a time scale on which the patch rotates, T_{self}, and a second time scale on which the strain rate experienced by the patch changes as the patch moves through the corner, T_{strain}. T_{strain} is relatively long compared with T_{self}; in Figure 13b the ratio of the time scales can be seen to be $T_{strain}/T_{self} \approx 5$. This separation of time scales is sufficient to lead to the phenomenon of adiabatic invariance [6].

If we view this problem as a patch of vorticity in a slowly varying strain field then the theory of adiabatic invariance states that, whilst the Hamiltonian associated with the motion can vary, there exists an adiabatic invariant that is constant to all orders in $\epsilon \equiv T_{self}/T_{strain}$. A first-order approximation to this adiabatic invariant is given by the action

$$J \equiv \oint p\, dq \quad \text{where} \quad p = \frac{\omega A^2}{16\pi}\frac{(r-1)^2}{r}, \quad q = 2\theta \tag{40}$$

here p and q are a pair of canonical variables and the integral is over one period of the motion. The variation of this action as the patch passes through the corner for the example given earlier is shown in Figure 14a. The presence of the adiabatic invariant means that the action before the interaction with the corner and the action after the interaction, and

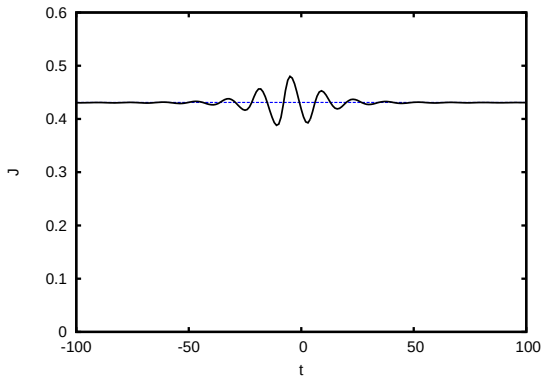

(a) Variation of action as the patch passes through the corner.

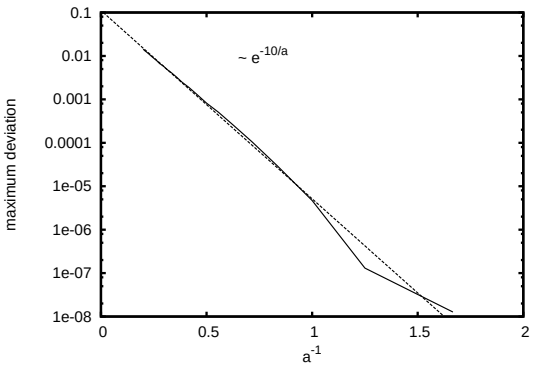

(b) Maximum deviation over all simulations with the same initial energy and action for a range of patch speeds a.

Figure 14

similarly the distance from the wall, should be the same to all orders. As we have no direct control over the time scales in the problem checking that the distance from the wall is the same to all orders in ϵ is a bit tricky. To get around this we instead consider the related (but unphysical) problem whereby the speed at which the patch centroid moves is changes by a factor a. In this new problem the separation of time scales is $T_{self}/T_{strain} = a\epsilon$; so if the patch centroid moves more quickly, $a > 1$, the strain experienced by the patch varies more quickly and consequently there is less of a separation between the two time scales, conversely if the patch moves more slowly, $a < 1$, there is more of a separation. To see that the distance from the wall is constant at all orders we look at how the change in distance from the wall varies as we vary a, see Figure 14b. As a is decreased there is a clear exponential decrease in the deviation corresponding to the adiabatic invariant begin constant at all orders.

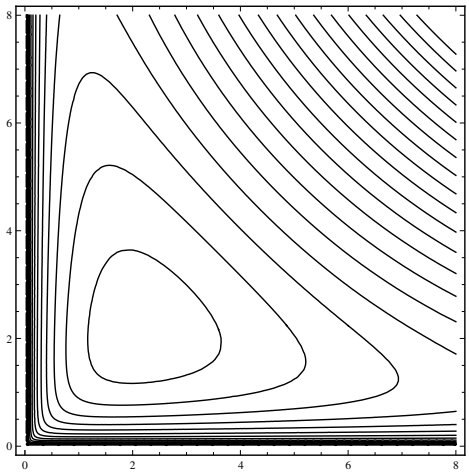

Figure 15: Path lines of point vortices in corner with background shear flow.

4.1 Corner trapping by an external flow

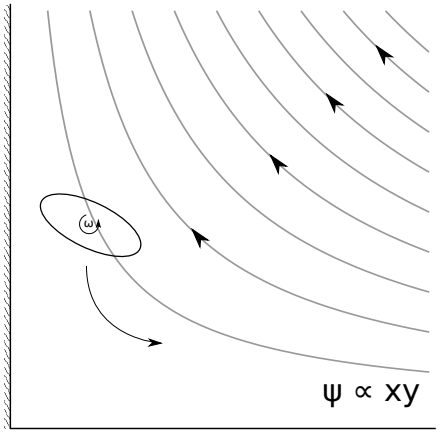

It is possible to add an external straining flow

$$\Psi = \beta xy \tag{41}$$

to the quarter-plane motion such that the vortex patch becomes trapped in the corner provided $\beta < 0$; the motion of point vortices in such a flow is shown in Figure 15. For elliptic vortex patches this results in the following extra term in the Hamiltonian:

$$H_\Psi = -\omega \left(\frac{\beta q_y}{2} + Axy \right). \tag{42}$$

Poincaré sections can be calculated for the resulting motion by plotting all solutions with a fixed value of β and a fixed energy H when they pass forwards through the plane

$\theta = 0$. The resulting Poincaré sections for the x-y plane are shown in Figure 16. Also shown by blue lines are the energetically allowable regions of the plane; the asymmetry here is due to the choice of plotting at $\theta = 0$.

For low values of H there is a region of closed streamlines and a second energetically allowable region near $y = 0$ where all patches extend indefinitely. As H is increased the boundaries of these two regions become closer together and at the same time we see the development of resonances in the central region (see $H = 0.25$). By $H = 0.275$ a 'sea of chaos' has emerged around the edge of the central region and at $H = 0.3$, by which time the two regions have merged together, this 'sea of chaos' extends into the region where all patches are indefinitely extended.

The reason that we are able to observe chaotic behaviour here is that the presence of the background straining flow is able to decrease the time scale upon which the vortex patch experiences a change in strain. Unfortunately the emergence of interesting behaviour for $H > 0.25$ also corresponds with the elliptic vortex patches intersecting with the boundaries of the quarter plane, thus the solutions shown become unphysical. So whilst this may still be an interesting mathematical problem we will not spend any more time analysing it here.

5 Application to more complicated geometries

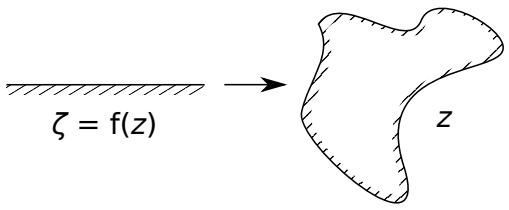

Everything that we've considered so far has been for a 'simple' geometry in which we have been able to construct the solution via the method of images. However the problems that we initially set out to look at featured more complicated geometries in which such methods can not be used. In this section we consider how to make use of conformal transformation techniques to tackle such geometries.

Conformal transformations are a powerful tool for dealing with irrotational flows as for such flows the stream function satisfies Laplace's equation

$$\nabla^2 \psi(z) = 0 \tag{43}$$

and under a conformal transformation $\zeta = f(z)$ such functions retain this property

$$\nabla^2 \psi(f^{-1}(\zeta)) = 0. \tag{44}$$

Thus we can find the flow in a complicated geometry by finding a map to a simple geometry and solving for the flow in that domain before transforming back. Furthermore such transformations (with a slight caveat) preserve the Hamiltonian; the slight caveat is that, if we have a flow with an infinite energy, such as that for a point vortex, we must take care

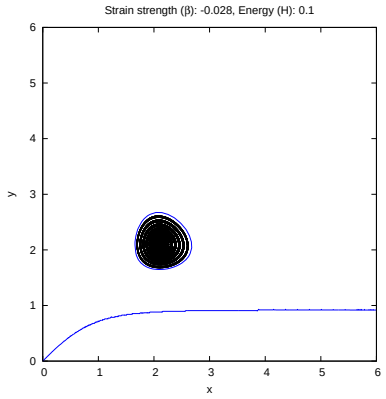

(a) $H = 0.1$

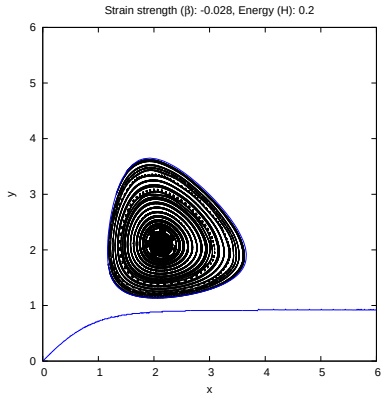

(b) $H = 0.2$

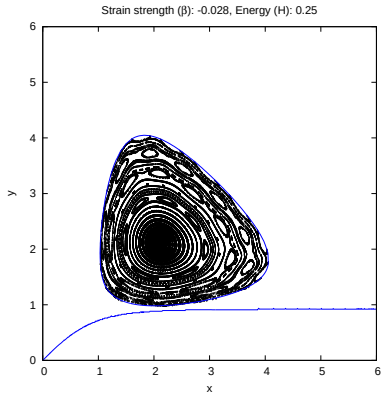

(c) $H = 0.25$

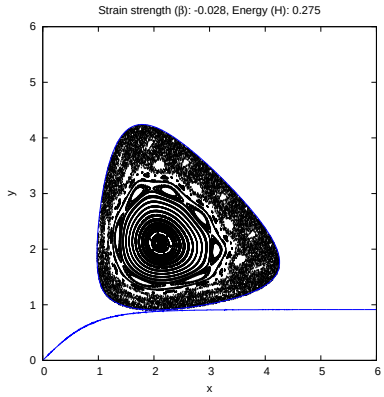

(d) $H = 0.275$

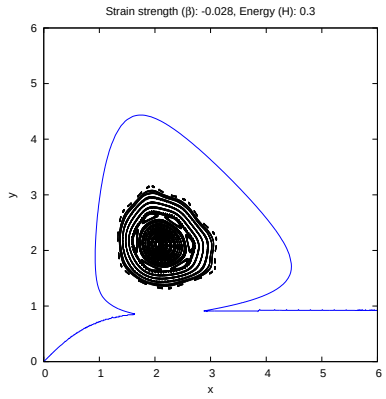

(e) $H = 0.3$

Figure 16: Poincaré sections in the x-y plane plotted when $\theta = 0$. The strength of the external strain is fixed at $\beta = -0.028$ and sections are shown for 5 values of the energy H.

over what happens to the 'zero' energy under the transformation. For point vortices Routh showed that the following correction was required

$$H(z) = \hat{H}(\zeta(z)) + \mathrm{Re}\left(\frac{\Gamma^2}{4\pi}\log(f')\right). \tag{45}$$

We would like to make use of conformal transformations to calculate the motion of elliptic vortex patches but if we conformally transform such a patch then we will be left with a non-elliptical patch of non-uniform vorticity for which we do not know how to calculate the flow! The solution is to observe that the Hamiltonian can be split into two parts: a self contribution, H_{self}, and an interaction with other vortex patches, H_{int}. The self-contribution does not care about the geometry so is easily calculated in the original geometry. The interaction term represents the energy due to a point vortex and quadrupole, of appropriate strength, located at the centroid of the patch. Such singularities transform nicely under a conformal transformation: a point vortex becomes a point vortex of the same strength and a quadrupole becomes a dipole and a quadrupole of different, but easily calculated, strengths.

Let z be the coordinate of the complicated geometry where the complex stream function is given by $\phi(z)$. Then consider a conformal transformation

$$\zeta = f(z) \qquad z = f^{-1}(\zeta) = F(\zeta) \tag{46}$$

which takes this complicated geometry to a simpler one with coordinate ζ and stream function $\Phi(\zeta)$. Now the stream function in the complicated geometry with a point vortex and quadrupole located at z_0 can be written as follows:

$$\phi(z) = \frac{1}{2\pi i}\left(A\log(z-z_0) - \frac{q}{2(z-z_0)^2}\right) + \phi_{z_0}(z). \tag{47}$$

In order to calculate H_{int} we need to find $\phi_{z_0}(z)$ and its first two derivatives up to sufficient accuracy for the elliptic model.

A point vortex in the ζ geometry behaves like $\log(\zeta-\zeta_0)$ and to find the corresponding behaviour in the z geometry we expand this in terms of z (all derivatives of f are evaluated at z_0)

$$\log(\zeta-\zeta_0) = \log(z-z_0) + \log f' + \frac{f''}{2f'}(z-z_0) + \frac{4f'''f' - 3f''^2}{24f'^2}(z-z_0)^2 + O((z-z_0)^3) \tag{48}$$

from which we see that a point vortex in one geometry corresponds to a point vortex of equal strength in the other geometry. Taking two derivatives with respect to z_0 then gives

$$\frac{f'^2}{(\zeta-\zeta_0)^2} + \frac{f''}{(\zeta-\zeta_0)} = (z-z_0)^{-2} + \frac{4f'''f' - 3f''^2}{12f'^2} + O((z-z_0)) \tag{49}$$

which tells us that a quadrupole in the z geometry leads to a both a dipole, $\hat{d}$, and a quadrupole, $\hat{q}$, in the ζ geometry

$$\hat{q} = f'^2 q, \qquad \hat{d} = \frac{f''q}{2}. \tag{50}$$

Then the flow in the ζ geometry can be written as

$$\Phi(\zeta) = \frac{1}{2\pi i}\left(A\log(\zeta-\zeta_0) - \frac{qf''}{2(\zeta-\zeta_0)} - \frac{qf'^2}{2(\zeta-\zeta_0)^2}\right) + \Phi_{\zeta_0}(\zeta) \tag{51}$$

where we assume that the geometry is sufficiently simple for us to be able to calculate $\Phi_{\zeta_0}(\zeta)$.

By conformal invariance $\phi(z) = \Phi(\zeta)$ and combining this with Equations (47) ,(48), (49) & (51) gives the following expression for $\phi_{z_0}(z)$ in which we have neglected terms of too higher order for the elliptic model:

$$\phi_{z_0}(z) = \frac{A}{2\pi i}\left(\log f' + \frac{f''}{2f'}(z-z_0) + \frac{4f'''f' - 3f''^2}{24f'^2}(z-z_0)^2\right) + \frac{q}{2\pi i}\frac{4f'''f' - 3f''^2}{24f'^2} \tag{52}$$

$$+\Phi_{\zeta_0}(\zeta_0) + \Phi'_{\zeta_0}(\zeta_0)f'(z-z_0) + \frac{\Phi'_{\zeta_0}(\zeta_0)f'' + \Phi''_{\zeta_0}(\zeta_0)f'^2}{2}(z-z_0)^2. \tag{53}$$

It follows that

$$\int \phi_{z_0}(z)\, dS = \frac{A^2}{2\pi i}\log f' + \frac{Aq}{2\pi i}\frac{4f'''f' - 3f''^2}{12f'^2} + A\Phi_{\zeta_0}(\zeta_0) + \frac{q}{2}(\Phi'_{\zeta_0}(\zeta_0)f'' + \Phi''_{\zeta_0}(\zeta_0)f'^2) \tag{54}$$

which upon multiplication by a factor of $-\frac{\omega^2}{2}$ gives us the relation between the interaction Hamiltonians in the two geometries

$$H_{int}(z,q) = \hat{H}_{int}(\zeta(z),\hat{d},\hat{q}) + \mathrm{Re}\left(\frac{(\omega A)^2}{4\pi}\log(f') + \frac{\omega^2 Aq}{4\pi}\frac{4f'''f' - 3(f'')^2}{12(f')^2}\right). \tag{55}$$

All that then remains is to add on the self-interaction term to obtain the full Hamiltonian for the motion in the complicated geometry

$$H(z,q) = H_{int}(z,q) + H_{self}(q). \tag{56}$$

5.1 Flow around an island

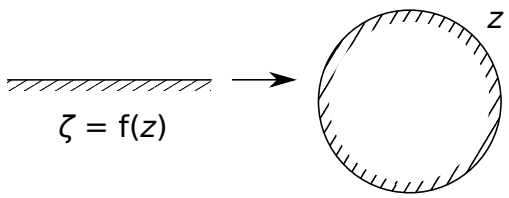

We illustrate this conformal mapping method by considering the evolution of a vortex patch around an island. In this case we can conformally transform back to a half-plane geometry via the following transformation:

$$z = \frac{\zeta + i}{\zeta - i}, \qquad \zeta = f(z) = i\frac{z+1}{z-1}. \tag{57}$$

The resulting dipole and quadrupole strengths in the simple geometry are then

$$\hat{d} = \frac{iq}{2}(\zeta - i)^3, \qquad \hat{q} = \frac{-q}{4}(\zeta - i)^4. \tag{58}$$

The interaction Hamiltonian in the simple geometry is much the same as that for motion above a coast (Equation (22)) but now with an added dipole contribution

$$\hat{H}_{int}(\zeta) = \frac{\omega^2}{4\pi} Re\left(A^2 \log(\zeta - \bar{\zeta}) + \frac{A(\hat{d} - \bar{\hat{d}})}{\zeta - \bar{\zeta}} - \frac{A(\hat{q} + \bar{\hat{q}})}{2(\zeta - \bar{\zeta})^2} \right). \tag{59}$$

Then applying the result of the earlier derivation (Equation (55)) we can calculate the interaction Hamiltonian in the original island geometry to be

$$H_{int} = \frac{\omega^2 A^2}{4\pi} \log(x^2 + y^2 - 1) - \frac{\omega^2 A}{4\pi} \frac{(x^2 - y^2)q_x + 2xyq_y}{(x^2 + y^2 - 1)^2}. \tag{60}$$

This Hamiltonian that we have just found corresponds to the case in which the island has a circulation equal and opposite to that of the vortex patch. This circulation is a constant of the motion (Kelvin's circulation theorem) and if we imagine that our vortex patch has been advected close to the island by some background flow then there is no reason to expect there to be any circulation around the island. The Hamiltonian for this no circulation case is easily found by placing a point vortex of opposite strength to the patch at the point in the ζ plane which is mapped to infinity ($\zeta = i$). The interaction Hamiltonian with this extra point vortex is still easily calculated and the result in the island geometry is

$$H_{int} = \frac{\omega^2 A^2}{4\pi} \log\left(1 - \frac{1}{x^2 + y^2}\right) - \frac{\omega^2 A}{4\pi} \frac{(x^2 - y^2)q_x + 2xyq_y}{(x^2 + y^2 - 1)^2} \frac{2x^2 + 2y^2 - 1}{(x^2 + y^2)^2}. \tag{61}$$

This zero-circulation Hamiltonian has a more rapid decay with distance from the island as we would expect.

As a consequence of the rotational symmetry of the island there is another constant of the motion, this is the angular impulse

$$\omega \int \mathbf{x} \cdot \mathbf{x} \, dS = \omega \left(A(x^2 + y^2) + \sqrt{q_x^2 + q_y^2 + \frac{A^4}{4\pi^2}} \right). \tag{62}$$

So, whilst the distance of the centroid to the island is able to move, the motion, like the case of a half-plane, is integrable.

An area for further investigation is what happens when we impose a background flow. Such a flow could cause the vortex patch to impact with the island and lead to the break up of the patch as observed in [15].

6 Motion around a pair of islands

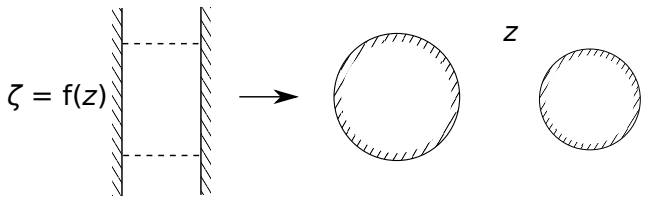

We're now in a position to consider one of the problems that we originally set out to consider: the motion of a vortex patch around a pair of islands. This problem was previously considered by Johnson and McDonald [8] for the case of a point vortex and they showed that the following conformal transformation

$$z = \frac{\sinh((\zeta+\beta)/2)}{\sinh((\zeta-\beta)/2)}, \qquad \zeta = f(z) = \log\left(\frac{\sinh((z+\beta)/2)}{\sinh((z-\beta)/2)}\right) \tag{63}$$

maps the $2\pi i$ periodic channel ($0 < \operatorname{Re}\zeta < \gamma$, $-\pi < \operatorname{Im}\zeta < \pi$) onto the exterior of two islands with the values of γ and β setting the relative sizes and separation of the two islands. The flow in this 'simple' geometry can be calculated via the method of images, where the required images are as shown in Figure 17. Johnson and McDonald show that for a point vortex in this geometry the resulting stream function is given by

$$\Phi(\zeta) = \frac{\kappa}{2\pi i}\log\left(\frac{\vartheta_1(i/2(\zeta-\zeta_0))}{\vartheta_1(i/2(\zeta+\bar{\zeta_0}))}\right) \tag{64}$$

where $\vartheta_1(\zeta)$ is the first Jacobi Theta function with nome $e^{-\gamma}$. Similar stream functions can be calculated for the dipole and quadrupole by taking the appropriate derivatives. For a dipole we get

$$\Phi(z) = \frac{-1}{2\pi i}\left[d\left(\frac{\mathcal{Z}(\pi)}{\pi}(z-z_0) + i\mathcal{Z}(i(z-z_0))\right) + \bar{d}\left(\frac{\mathcal{Z}(\pi)}{\pi}(z+\bar{z_0}) + i\mathcal{Z}(i(z+\bar{z_0}))\right)\right] \tag{65}$$

where $\mathcal{Z}(\zeta)$ is the Weierstrass zeta function with half periods π and γi, and for a quadrupole

$$\Phi(z) = \frac{1}{4\pi i}\left[q\left(\frac{\mathcal{Z}(\pi)}{\pi} + \wp(i(z-z_0))\right) - \bar{q}\left(\frac{\mathcal{Z}(\pi)}{\pi} + \wp(i(z+\bar{z_0}))\right)\right] \tag{66}$$

where $\wp(\zeta)$ is the Weierstrass elliptic function of the same half periods. From these functions it is relatively easy to construct the function Φ_{z_0} for the stream function due to the appropriate point vortex, dipole and quadrupole combination with the singularities at z_0 subtracted off. Using this we can construct the interaction Hamiltonian

$$\begin{aligned}\hat{H} =& \frac{\omega^2}{4\pi}\operatorname{Re}\left(A^2\log(\vartheta_1(\frac{i}{2}(\zeta+\bar{\zeta})) + A(d+\bar{d})\left(\frac{\mathcal{Z}(\pi)}{\pi}(\zeta+\bar{\zeta}) + i\mathcal{Z}(i(\zeta+\bar{\zeta}))\right)\right.\\ &+ \frac{A(q+\bar{q})}{2}\wp(i(\zeta+\bar{\zeta})) + \frac{A(\bar{q}-q)}{2}\frac{\mathcal{Z}(\pi)}{\pi}\\ &+ 2A^2\log\left(\frac{\vartheta_1(\frac{i}{2}(\zeta-\beta))}{\vartheta_1(\frac{i}{2}(\zeta+\beta))}\right) + 2Ad\left(-2\beta\frac{\mathcal{Z}(\pi)}{\pi} + i\mathcal{Z}(i(\zeta-\beta)) - i\mathcal{Z}(i(\zeta+\beta))\right)\\ &\left.+ Aq\big(\wp(i(\zeta-\beta)) - \wp(i(\zeta+\beta))\big)\right).\end{aligned} \tag{67}$$

Here, as with the case of a single island, we have placed a point vortex of opposite strength at the point that gets mapped to infinity ($\zeta = \beta$) to ensure that the circulation around both islands is zero.

Using the above Hamiltonian we were able to calculate some numerical solutions of an elliptic vortex patch travelling around a pair of islands; the path of the centroid in one

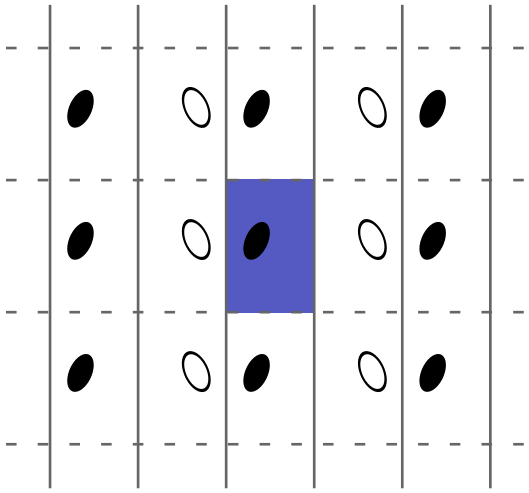

Figure 17: Image system for periodic strip. White regions of vorticity have opposite sign to the original patch.

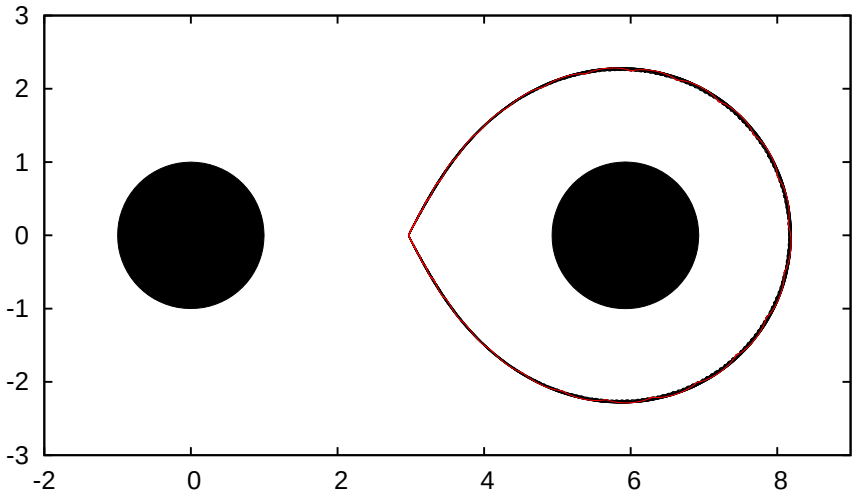

Figure 18: Motion of an initially circular patch around a pair of islands as represented by the position of its centroid. $O(10)$ orbits are shown with the first one in red.

such simulation is shown in Figure 18. We were not able to find any solutions that flipped from going around one island to going around the other, a likely reason for this is that the adiabatic invariance that we found back in the quarter-plane problem is still at work here and consequently the motion is in some sense close to being integrable. We also found that, whilst this elliptic model is much faster than calculating the full solution would be, it is still quite slow to calculate due to the relatively large time taken to calculate the complicated Hamiltonian.

7 Conclusion

The elliptic moment model of Melander, Zabusky & Stysek provides a powerful method of analysing the interaction of ocean vortex patches with coastal boundaries, and appears to do a good job of predicting the motion even outside the regime where it is technically applicable. Under this simple model the problem of motion along a coast reduces to that of an elliptic patch in constant strain as analysed by Kida leading to three distinct types of motion depending on the distance of the centroid above the wall and the shape of the patch. The application of a periodic shear flow, as might arise from a background tidal flow, gives rise to chaotic behaviour which could play an important role in causing the break up of vortex patches.

On investigating more complicated geometries where we might expect to find chaotic behaviour we instead find the presence of an adiabatic invariant due to the separation of time scales between the rotation of the patch and the longer time scale on which the strain experience by the patch varies. In the case of motion in a quarter-plane the addition of a background flow was able to reduce this separation and produce chaotic, although unfortunately unphysical, behaviour.

We also demonstrated that, through the use of conformal mapping techniques, it is possible to calculate the motion of an elliptical vortex patch in more complicated geometries. This technique was applied to both the case of motion around a single island and motion around a pair of islands. In the former the motion was found to still be integrable and in the latter the probable presence of the adiabatic invariant meant that the expected chaotic flipping of which island the patch orbited was not observed to occur.

8 Future directions

There are a wide range of other problems involving the interaction of elliptic vortex patches with boundaries that we have the machinery to tackle. These include the problem of motion of a vortex patch past a gap in the coast line which was one of the original aims of this project that we ran out of time to investigate. Another possibility is looking at the interaction of a patch with an island in the presence of a background flow, this has been observed to break up actual vortex patches in the ocean. The adiabatic invariance observed could also be investigated further by looking at the motion of a patch above a coastline with more rapidly varying geometry.

9 Acknowledgements

I would like to thank Ted Johnson and Phil Morrison for proposing this project and for their continued support throughout the summer. Further thanks go to Fabian Waleffe and Rich Kerswell for two weeks of enlightening lectures, to Norm Lebovitz and Phil Morrison for all their organisational work, and to the other Fellows for making it a thoroughly enjoyable ten weeks.

References

[1] G. Batchelor, *An introduction to fluid dynamics*, Cambridge mathematical library, Cambridge University Press, 1967.

[2] M. V. Berry, *Regular and Irregular Motion*, in Topics in Nonlinear Mechanics, S. Jorna, ed., 1978, pp. 16–120.

[3] T. E. Dowling and A. P. Ingersoll, *Jupiter's Great Red SPOT as a shallow water system*, J. Atmos. Sci., 46 (1989), pp. 3256–3278.

[4] D. G. Dritschel, *The stability of elliptical vortices in an external straining flow*, J. Fluid Mech., 210 (1990), pp. 223–261.

[5] D. Goldman and R. J. McCann, *Chaotic response of the 2d semi-geostrophic and 3d quasi-geostrophic equations to gentle periodic forcing*, Nonlinearity, 21 (2008), p. 1455.

[6] J. Henrard, *The adiabatic invariant in classical dynamics*, in Dynamics Reported, Springer Verlag, 1993, pp. 117–235.

[7] E. R. Johnson and N. R. McDonald, *The motion of a vortex near a gap in a wall*, Phys. Fluids, 16 (2004), pp. 462–469.

[8] ——, *The motion of a vortex near two circular cylinders*, Proc. Roy. Soc. London, 460 (2004), pp. 939–954.

[9] S. Kida, *Motion of an elliptic vortex in a uniform shear flow*, J. Phys. Soc. Japan, 50 (1981), pp. 3517–3520.

[10] G. Kirchhoff, *Vorlesungen über mathematische Physik.*, Mechanik, Leipzig: Teubner, 1876.

[11] A. E. H. Love, *On the stability of certain vortex motions*, Proc. London Math. Soc., s1-25 (1893), pp. 18–43.

[12] S. P. Meacham, P. J. Morrison, and G. R. Flierl, *Hamiltonian moment reduction for describing vortices in shear*, Phys. Fluids, 9 (1997), pp. 2310–2328.

[13] M. V. Melander, N. J. Zabusky, and A. S. Styczek, *A moment model for vortex interactions of the two-dimensional Euler equations. I - Computational validation of a Hamiltonian elliptical representation*, J. Fluid Mech., 167 (1986), pp. 95–115.

[14] P. L. Richardson, R. E. Cheney, and L. V. Worthington, *A Census of Gulf Stream Rings, Spring 1975*, J. Geophys. Res., 83 (1978), pp. 6136–6144.

[15] P. L. Richardson and A. Tychensky, *Meddy trajectories in the Canary Basin measured during the SEMAPHORE experiment, 1993-1995*, J. Geophys. Res., 1032 (1998), pp. 25029–25046.

[16] N. J. Zabusky, M. H. Hughes, and K. V. Roberts, *Contour dynamics for the euler equations in two dimensions*, J. Comput. Phys., 135 (1997), pp. 220–226.